

Model of Inclusion Evolution During Calcium Treatment in the Ladle Furnace



YOUSEF TABATABAEI, KENNETH S. COLEY, GORDON A. IRONS,
and STANLEY SUN

Calcium treatment of steel is typically employed to modify alumina inclusions to liquid calcium aluminates. However, injected calcium also reacts with the dissolved sulfur to form calcium sulfide. The current work aims to develop a kinetic model for the evolution of oxide and sulfide inclusions in Al-killed alloyed steel during Ca treatment in the ladle refining process. The model considers dissolution of the calcium from the calcium bubbles into the steel and reduction of calcium oxide in the slag to dissolved calcium. A steel–inclusion kinetic model is used for mass transfer to the inclusion interface and diffusion within the calcium aluminate phases formed on the inclusion. The inclusion–steel kinetic model is then coupled with a previously developed steel–slag kinetic model. The coupled inclusion–steel–slag kinetic model is applied to the chemical composition changes in molten steel, slag, and evolution of inclusions in the ladle. The result of calculations is found to agree well with an industrial heat for species in the steel as well as inclusions during Ca treatment.

<https://doi.org/10.1007/s11663-018-1266-z>

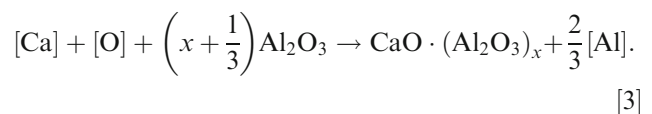
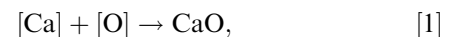
© The Minerals, Metals & Materials Society and ASM International 2018

I. INTRODUCTION

THE requirements for the production of superior-quality steel for specific applications have led to the development of various secondary steelmaking processes. Refining of the steel before casting is carried out in ladles *via* several operations, namely deoxidation, desulphurization, alloy addition, removal of inclusions, and control of inclusion shape, size, number, and composition. Ineffective elimination and/or modification of nonmetallic inclusions during secondary treatment of steel can cause nozzle blockage during continuous casting^[1] and quality issues in the cast product.^[2,3] Calcium treatment is the most common approach to modify nonmetallic inclusions. Ca additions modify solid alumina to globular liquid CaO–Al₂O₃ (CA_x) inclusions and magnesium aluminate spinel inclusions to calcium–magnesium aluminates. This results in not only improved castability, but also minimization of inclusion-related surface defects, enhancing the machinability of the final product at high

cutting speeds and decreasing of the susceptibility of high-strength low-alloy and pipeline steels to hydrogen-induced cracking.^[4] Ca treatment can also be utilized for desulphurization to very low levels,^[5] but it may also result in the formation of deleterious CaS inclusions. In summary, calcium treatment is effective in alleviating nozzle clogging caused by alumina inclusions, but the treatment should be done cautiously.

Calcium is usually introduced to the steel by steel-clad Ca wire injection. The boiling point of calcium (1480 °C) is lower than steelmaking temperature (~ 1600 °C), and thus when calcium is added to liquid steel, calcium bubbles form, from which some calcium dissolves into the steel. Actually, most of the injected calcium escapes to the atmosphere and the recovery in industry is usually less than 30 pct.^[6] The dissolved calcium reacts with dissolved oxygen, sulfur, and alumina inclusions by the following reactions:



In spite of the fact that since the 1990s, many studies have been conducted to understand the mechanism and

YOUSEF TABATABAEI, KENNETH S. COLEY, and GORDON A. IRONS are with the Department of Materials Science and Engineering, Steel Research Centre, McMaster University, 1280 Main St W., Hamilton, ON, L8S4L7, Canada. Contact e-mail: tabatasy@mcmaster.ca STANLEY SUN is with the ArcelorMittal Global R&D-Hamilton, 1330 Burlington St E., Hamilton, ON, L8N3J5, Canada.

Manuscript submitted November 1, 2017.

Article published online April 24, 2018.

kinetics of alumina inclusion modification by calcium,^[7–11] some uncertainties remain in the literature. Previous work by the authors developed a fundamental multi-layer growth model^[12] and concluded that, for the case of a fixed calcium content in the steel, the rate of supply of calcium to the alumina inclusion is the rate-controlling step for modification. This work also showed that changing the fixed concentration of dissolved calcium had a profound effect on the rate of transformation. The latter result suggested that the rate of supply of calcium to the steel relative to the abundance of inclusions will also have a significant effect on transformation rate.

There has been a number of attempts to model reaction kinetics of steelmaking processes. Lu *et al.*^[7] were the first researchers to model the kinetics of evolution of oxide and sulfide inclusions during calcium treatment based on their experiments in 40 kg steel heats. They assumed fast diffusion within the inclusions and fast reaction at the interfaces and developed a mathematical model for inclusion evolution which offered very reasonable agreement with the experimental data. Visser *et al.*^[10] developed a model to describe the change of the concentration, composition, and size of the inclusions in the liquid steel during calcium treatment. They divided the steel bath into two reaction zones: one including the plume zone with high calcium and low oxygen and the other representing the rest of the liquid steel which had low calcium and somewhat higher oxygen. In their model, it was assumed that dissolved calcium and oxygen react with Al_2O_3 to form calcium aluminate with gradually increasing CaO fraction. If oxygen activity was sufficiently low, dissolved calcium and sulfur reacted at the surface of the particle to form CaS. In addition, it was assumed that mass transfer of the solutes to the particle surface was the rate-controlling step for the formation reactions of CaO, CaS, and Al_2O_3 .

Graham and Irons^[13] simulated the ladle metallurgy process using a multicomponent coupled slag–metal kinetic model which assumed that rates were mixed transport controlled in the metal and slag phases. They investigated formation of spinel inclusions as a function of $(\text{MnO} + \text{FeO})$ content of the slag and also calcium aluminate according to calcium and oxygen content of the steel, but did not provide a mathematical model to describe change of composition of the inclusions. Nevertheless, it was clear that there was close coupling between reactions at the slag–metal interface and the transformation of inclusions. Later on, this model was coupled to the particle model for transformation of alumina to magnesium aluminate spinel inclusions by Galindo *et al.*^[14] and a similar conclusion was found.

A coupled kinetic model to describe industrial operations in the ladle furnace was proposed by Harada *et al.*^[15] The model considered interaction between steel, slag, and inclusions originating from slag entrainment, as well as by deoxidation reactions, dissolution of the refractory into the slag, and formation, flotation, and agglomeration of inclusions. The activities of the individual components for a given oxide system of the inclusions were fixed and the composition change of

inclusion was assumed to be controlled by mass transfer within the boundary layer. However, they did not consider formation of sulfide inclusions in their model and determined several model parameters to fit the model results with plant data or experimental results which should be modified if the operational conditions are different.

In a further study, Harada *et al.*^[16] employed the same kinetic model to that in Reference 15 to simulate the reactions during the ladle refining process and to clarify the mechanism of compositional changes in inclusions. Experiments were also conducted to validate the model. They observed that the inclusion composition gradually changed from Al_2O_3 to $\text{MgO}\cdot\text{Al}_2\text{O}_3$ after the addition of Mg, and the inclusions originating from slag remained in the steel for the duration of the experiment (30 minutes).

Recently, Kumar and Pistorius^[17] used FactSage macros to simulate steel–slag and steel–inclusion reaction kinetics and quantify rate of calcium transfer from slag to steel to inclusions that may modify alumina inclusions in laboratory scale experiments. They assumed that the mass transfer coefficient in the steel, k_{steel} , was 10 times larger than in the slag, k_{slag} , and experimental data were used to determine $k_{\text{steel}} \times A_{\text{interface}}$.

More recently Shin *et al.*^[18] employed the effective equilibrium reaction zone model to calculate the evolution of inclusions during the secondary refining processes. In their model, the reaction zone volume is defined per unit step for metal and slag phase which is dependent on the “effective reaction zone depth” in each phase. The effective reaction zone depth was fitted from the mass transfer coefficients in metal and slag phase which was determined experimentally.

Because of the close coupling between the slag–metal reactions and inclusion transformation, a model is required that considers steel–slag reaction and steel–inclusion reactions as well as the reactions involved in adding reagents to the steel. The present work proposes a kinetic model for modification of inclusions which considers all possible rate-controlling steps including reduction of calcium from the slag and calcium bubble dissolution, mass transfer through the boundary layer, and diffusion within the product layer. The model also takes into account simultaneous formation and competition for the calcium from alumina and sulfide inclusions. Coupling the inclusion model with a multicomponent steel–slag model^[19] allows tracking of the trajectory of slag, metal, and inclusion composition during ladle treatment.

II. DESCRIPTION OF THE MODEL

To develop a model for the ladle furnace, including calcium treatment, the transfer of species between slag, metal, and inclusions as well as the reaction of additions such as calcium must be considered. Therefore, the following interactions are included in the model: (a) the kinetics and mechanism of calcium supply to the steel, (b) mechanism and kinetics of inclusion modification

and competition for calcium between inclusions, namely calcium sulfide, calcium oxide, and calcium aluminate, and (c) slag–metal reactions that will modify the steel composition and alter the balance of competition between different reactions. A schematic diagram of the ladle furnace and the ongoing reactions between slag, steel, and inclusions during calcium treatment is shown in Figure 1.

A. Calcium Injection

To include the injection and dissolution rate of calcium into the steel, a model developed by Lu *et al.*^[7] was adopted in the present work. They found that when calcium dissolves by diffusion through the boundary layer surrounding a calcium bubble, it reacts with diffusing oxygen and sulfur at the reaction plane to form CaO and CaS, causing the calcium concentrations to drop to a very low level as shown in Figure 2.

The steep concentration gradient accelerates the mass transfer of calcium, and hence an enhancement factor E is incorporated into the dissolution equation [4]. It is worth noting that while the presence of dissolved sulfur and oxygen significantly enhances the rate of pickup of total calcium in the steel, it actually slows the rate of calcium dissolution. This is apparent in Figure 2 if one considers the very low calcium concentration gradient between the reaction plane and the bulk steel.

Therefore, the enhanced dissolution rate of calcium is

$$\frac{dX_{Ca}}{dt} = k_{Ca,L} A_{B,L} \frac{E}{E-1} (X_{Ca,r} - X_{Ca}), \quad [4]$$

where X_{Ca} is the mole fraction of dissolved calcium, $k_{Ca,L}$ is the mass transfer coefficient of calcium through boundary layer to the steel, $A_{B,L}$ is the interfacial area of calcium bubbles per unit volume of steel,

$X_{Ca,r}$ is the mole fraction of calcium at the reaction plane, and E is the enhancement factor defined by Eq. [5]:

$$E = 1 + \frac{D_O X_O + D_S X_S}{D_{Ca} X_{Ca,b}}, \quad [5]$$

where D_O , D_S , and D_{Ca} represent the diffusivities in steel of O, S, and Ca, respectively, X_O and X_S are the mole fractions of dissolved O and S in bulk steel, and $X_{Ca,b}$ is the mole fraction of calcium at the bubble–steel interface at saturation. By reaction of oxygen and sulfur with calcium, oxide and sulfide inclusions form in the injection zone.

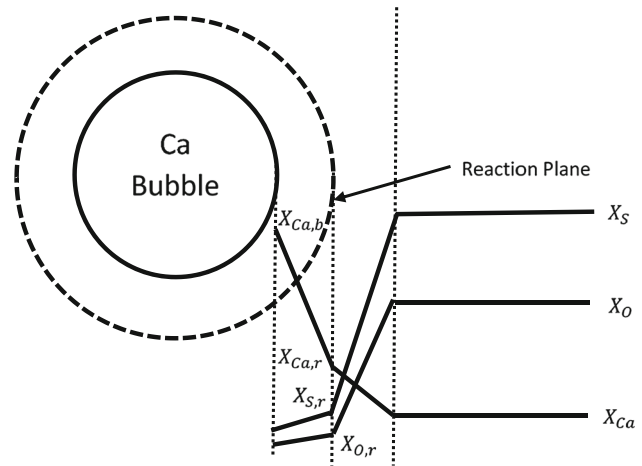


Fig. 2—Schematic diagram of the calcium dissolution, redrawn based on Ref. [20].

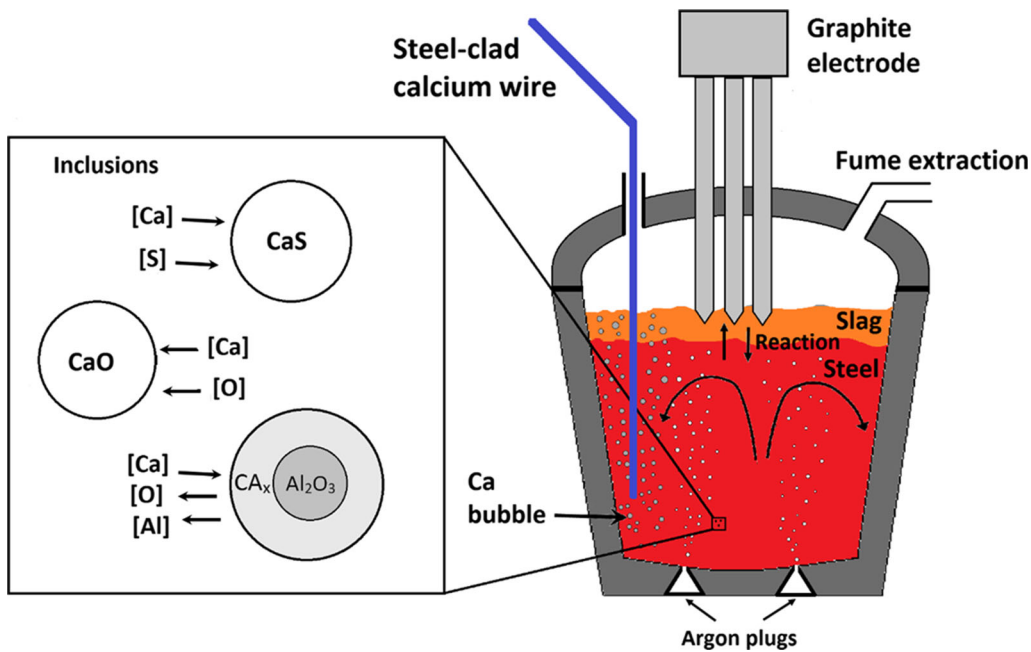


Fig. 1—Schematic diagram of a ladle furnace and the reactions between slag, metal, and inclusions.

B. Steel–Inclusion Reactions

When calcium is injected into the steel, alumina particles transform to calcium aluminate and CaO and CaS form. All of these inclusions compete for the available calcium. To calculate the rate of inclusion evolution, it is necessary to consider all the kinetic steps. Figure 3 shows a schematic diagram of expected concentration gradient of Ca, Al, O, and S among bubble, steel, and inclusions. The dissolving calcium reacts with diffusing oxygen and sulfur to form calcium oxide and calcium sulfide inclusions. The dissolved calcium transforms alumina inclusions to calcium aluminate. The authors recently developed a multi-layer model to describe the inclusion transformation which included all the possible solid phases that could form in the Al_2O_3 -CaO system.^[12] This model demonstrated that the overall transformation was controlled by a combination of transport of calcium to the bulk steel and transport of calcium from the steel to and within the inclusions. Therefore, in the current work, a shrinking core model^[21] based on liquid calcium aluminate forming directly from alumina is assumed for the transformation. The dissolved calcium can also react with dissolved oxygen and sulfur to form secondary calcium oxide and calcium sulfide inclusions depending on the O, S, and Ca content of the steel. The assumptions of the model are as follows:

- At the start of the process, a very thin layer of liquid CA_x is assumed to exist at the surface of alumina inclusions.
- Chemical reactions are fast relative to mass transport processes, due to the high temperature, so equilibrium is attained at all interfaces.
- Mass transfer within liquid CA_x is mathematically described by quasi steady-state counter molecular diffusion of CaO and Al_2O_3 through the product

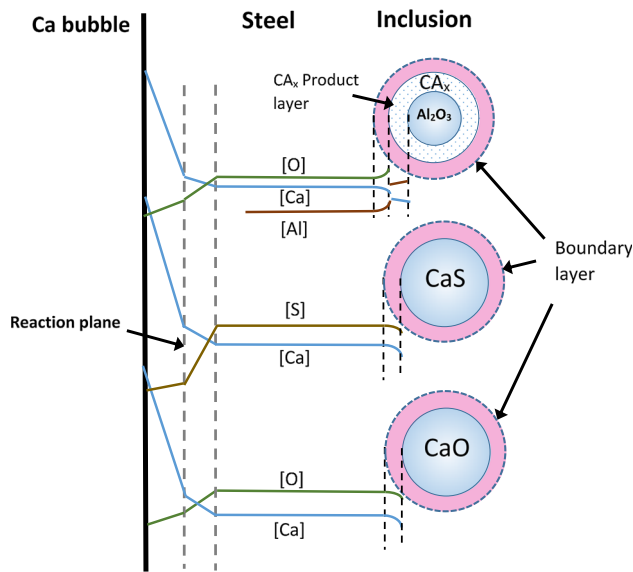


Fig. 3—Schematic diagram of reactions and transfer of species in the steel and inclusions.

layers. While this is a legitimate phenomenological treatment, the authors recognize that the mechanism and actual diffusing species may be more complex.

- The molten steel is well mixed, so there is a uniform concentration of dissolved species and inclusions in the steel.
- An initial and constant number of alumina inclusions are assumed at the beginning of injection. The number is taken from the scanning electron microscopy (SEM) analysis of the steel. The size of alumina inclusions is chosen to match that found by SEM. Hence, the model includes the following steps:
 - Dissolution of calcium from the gas bubble–steel interface into the bulk steel.
 - Transfer of the dissolved calcium or other solutes through the boundary layer between the bulk steel and inclusion interface.
 - Diffusion of calcium from the steel–inclusion interface through the product layer to the alumina core.
 - Chemical reaction of the calcium with alumina.

It is worth mentioning that magnesium-aluminum spinel inclusions are also modified by calcium to calcium-magnesium aluminate inclusions. There has been number of studies on the modification of spinel inclusions,^[22–24] but modification of spinel inclusion is not considered in the present work. The authors are currently working to include modeling of spinel transformation by calcium treatment with the current model.

1. Interfacial concentrations

The rate of alumina inclusion evolution is calculated by coupling mass balance at the inclusion–steel interface with local thermodynamic equilibrium. In the case of modification of alumina inclusions by calcium, the mass balance for calcium, aluminum, and oxygen leads to the following equations:

$$N_{\text{Ca}} = N_{\text{CaO}}, \quad [6]$$

$$N_{\text{Al}} = 2N_{\text{Al}_2\text{O}_3}, \quad [7]$$

$$N_{\text{O}} = N_{\text{CaO}} + 3N_{\text{Al}_2\text{O}_3}, \quad [8]$$

where N_i , the mass transfer rate of species i through the boundary layer from the bulk steel to the surface of a spherical particle, can be described by the following equation:

$$N_i = 4\pi r^2 \cdot k_{m,i} C_{v,m} (X_i^b - X_i^*), \quad [9]$$

where $k_{m,i}$ is the mass transfer coefficient across the boundary layer, r is the particle radius, $C_{v,m}$ is the molar density of the steel, X_i^b is the mole fraction of species i in the bulk steel, and X_i^* is the mole fraction of species i at the interface. From dimensionless analysis, $k_{m,i}$ is obtained using the Sherwood number defined as

$$Sh = \frac{k_{m,i}d}{D_i}, \quad [10]$$

where Sh is the Sherwood number, d is the particle diameter, and D_i is the diffusion coefficient of the species i in the steel. For small spherical particles, the Sherwood number may be assumed to be equal to 2.^[25,26]

Mass transfer within the alumina inclusion is assumed to occur by quasi steady-state, counter molecular diffusion of CaO and Al₂O₃, through the liquid calcium aluminate. The mass transfer rates of CaO and Al₂O₃ are driven by the concentration gradient. Molar flow of species i in the liquid product layer can be described by the following equation^[25]:

$$N_i = \left(\frac{4\pi r_{ex} r_{in}}{r_{ex} - r_{in}} \right) (C_v D_i) (X_i^{ex} - X_i^{in}), \quad [11]$$

where r_{ex} and r_{in} are exterior and interior radius of the product layer, respectively. C_v is the molar density of the liquid layer, D_i is the diffusivity of species i , and X_i^{ex} and X_i^{in} are mole fraction of species i at exterior and interior radius, respectively.

Thermodynamic equilibrium at the inclusion–steel interface is obtained considering simultaneous deoxidation equilibria of Ca and Al in steel with the Al₂O₃ and CaO components in the calcium aluminate phase according to the following reactions.

$$[Ca] + [O] = (CaO)_{inc},$$

$$K_{CaO} = \frac{a_{CaO}}{\left(\frac{f_{Ca} X_{Ca}^{*} n_T MW_{Ca} 100}{St_{Mass}} \right) \left(\frac{f_{O} X_{O}^{*} n_T MW_{O} 100}{St_{Mass}} \right)}, \quad [12]$$

$$2[Al] + 3[O] = (Al_2O_3)_{inc},$$

$$K_{Al_2O_3} = \frac{a_{Al_2O_3}}{\left(\frac{f_{Al} X_{Al}^{*} n_T MW_{Al} 100}{St_{Mass}} \right)^2 \left(\frac{f_{O} X_{O}^{*} n_T MW_{O} 100}{St_{Mass}} \right)^3}, \quad [13]$$

where f_i represents activity coefficient of species i with respect to 1 wt pct standard state, MW_i is the molar weight, n_T is total number of moles of steel, and St_{Mass} is total mass of the steel.

For the sake of simplicity in modeling, the activities $a_{Al_2O_3}$ and a_{CaO} in the Al₂O₃–CaO system are fitted to a sigmoidal function using values calculated by FactSage 6.4 software (FT Oxide database) at 1873 K.^[27,28] The values used for oxidation equilibrium constants are $K_{CaO} = 1.2 \times 10^9$ ^[29], $K_{Al_2O_3} = 3.16 \times 10^{12}$ ^[30] and $K_{CaS} = 1.7 \times 10^7$.^[31]

2. Inclusion evolution

Modification of alumina inclusions according to the phase diagram is shown in Figure 4. First, a layer of calcium aluminate forms on the surface of the alumina core. The modification continues with shrinkage of alumina core and growth of the product layer. At this stage, the composition of calcium aluminate produced is close to that in equilibrium with alumina. As the core is

consumed, if calcium injection continues, the modification proceeds by increasing the mole fraction of CaO in the calcium aluminate inclusion. When the composition of liquid calcium aluminate reaches the CaO saturation composition, it is assumed that a layer of CaO precipitates on the outer surface of the inclusion hindering further modification (see Figure 4). After this stage, more calcium injection results in increasing thickness of the CaO layer.

The change of the radius of the alumina core can be calculated by considering the relation between molar flux and volume:

$$\frac{dV}{dt} = \frac{dV}{dn} \times \frac{dn}{dt}. \quad [14]$$

By substituting,

$$4\pi r^2 \frac{dr_{Al_2O_3}}{dt} = \frac{MW_{Al_2O_3}}{\rho} \times N_{Al_2O_3}, \quad [15]$$

where $N_{Al_2O_3}$ is number of mole of Al₂O₃ leaving the alumina core per unit time which is the sum of the alumina reacting with CaO to form CA_x and alumina transferred through the product layer to dissolve in the steel in the form of aluminum. After substitution and rearrangement, one can obtain

$$4\pi r^2 \frac{dr_{Al_2O_3}}{dt} = \frac{MW_{Al_2O_3}}{\rho} \times \left(\vartheta' N_{Ca} + \frac{1}{2} N_{Al} \right), \quad [16]$$

where ϑ' defines the composition of the liquid calcium aluminate in thermodynamic equilibrium with alumina at 1600 °C according to phase equilibria. N_{Ca} and N_{Al} are calculated using Eq. [9]. The inclusion composition is calculated from the calcium aluminate and alumina core diameters.

After the core is consumed, modification can continue by further dissolution of calcium in calcium aluminate inclusions and thereby increasing the CaO fraction. Change of composition can be calculated as follows:

$$X_{Al_2O_3} = \frac{n_{Al_2O_3}}{n_{Al_2O_3} + n_{CaO}} \quad \text{and} \quad X_{CaO} = 1 - X_{Al_2O_3}, \quad [17]$$

where

$$\frac{dn_{Al_2O_3}}{dt} = \frac{1}{2} N_{Al} \quad \text{and} \quad \frac{dn_{CaO}}{dt} = N_{Ca}. \quad [18]$$

3. Dissolved species

Change of the dissolved species due to the injected calcium and steel–inclusion reaction can be calculated by considering mass balance. For calcium

$$\begin{aligned} \frac{dX_{Ca}}{dt} = & k_{Ca,L} A_{B,L} \frac{E}{E-1} (X_{Ca,r} - X_{Ca}) \\ & - k_{Ca,CA_x} A_{CA_x} (X_{Ca} - X_{CA_x}^i) - k_e A_e (X_{Ca} - 0), \end{aligned} \quad [19]$$

where the first term on the RHS shows the calcium dissolution rate through the bubble/steel interface to the steel, including the enhancement factor. The

second terms describe transfer of calcium to the CA_x inclusions and the last term represents evaporation of calcium from the surface of the steel melt. Mass transfer coefficients for inclusions are calculated using Eq. [10] assuming the Sherwood number equals 2. The evaporation rate constant k_e is obtained from the work of Lu *et al.*^[7] Similar equations can be written for Al, S, and O as follows:

$$\frac{dX_{Al}}{dt} = -k_{Al,CA_x} A_{CA_x} (X_{Al} - X_{Al,CA_x}^i), \quad [20]$$

$$\frac{dX_O}{dt} = -k_{O,L} A_{B,L} \frac{E}{E-1} (X_O - X_{O,r}) - (k_{O,CA_x} A_{CA_x}) (X_O - X_{O,CA_x}^i), \quad [21]$$

$$\frac{dX_S}{dt} = -k_{S,L} A_{B,L} \frac{E}{E-1} (X_S - X_{S,r}). \quad [22]$$

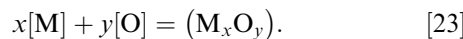
By solving these four differential equations, change of concentration of dissolved species due to interaction with inclusions can be calculated. Inspection of Figure 2 shows that the first term in Eqs. [21] and [22], respectively, represent the oxygen and sulfur consumed in forming oxide and sulfide inclusions.

C. Slag–Metal Reaction

In the present work, the multicomponent kinetic model of Graham and Irons^[13] described in greater detail in Reference 19 was used to calculate the effect of steel–slag reactions during ladle processing. The model is based on a the mixed coupled reaction model proposed by Robertson *et al.*^[32] and developed to describe dephosphorization and deoxidation.

The model proposed by Robertson *et al.*^[32] assumed that the rates are controlled by multicomponent transport in both metal and slag. Moreover, it was assumed that chemical reactions are sufficiently fast such that there exists local equilibrium at the slag–metal interface between elements and their oxides and sulfides.

A general reaction between the oxide in the slag and the respective species in the steel is



The equilibrium constant for the reaction at the interface is

$$K_{M_xO_y} = \frac{a_{M_xO_y}}{\left[\frac{f_M X_M^{n_T} MW_M 100}{St_{Mass}} \right] \left[\frac{f_O X_O^{n_T} MW_O 100}{St_{Mass}} \right]}, \quad [24]$$

where f_i are the activity coefficients for species i in the steel with respect to 1 wt pct standard state at the slag–steel interface, and X_i^* are the molar fractions of the respective species at the slag–steel interface. The activities of the components in the slag are calculated using the cell model formalism.^[32]

Considering transport of species from the bulk phases to the interface, the mass balance at the interface takes the form:

$$k_m^M C_{v_m} (X_M^b - X_M^*) = k_{sl}^{M_xO_y} C_{v_{sl}} (X_{M_xO_y}^* - X_{M_xO_y}^b), \quad [25]$$

where C_{v_m} and $C_{v_{sl}}$ are the molar density of the metal and slag phase, respectively; k_m^M and $k_{sl}^{M_xO_y}$ are the mass transfer coefficients in the metal and slag phase, respectively. By coupling all the mass transport equations with the overall balance of oxygen and equilibria at the interface then solving the system of nonlinear equations, the interfacial concentrations are calculated.

$$k_m^O C_{v_m} (X_O^b - X_O^*) = \sum_{i=1}^n y_i k_{sl}^{M_xO_y} C_{v_{sl}} (X_{M_xO_y}^* - X_{M_xO_y}^b). \quad [26]$$

The change of concentration in the bulk steel and slag due to steel–slag reaction is calculated using the following equations:

$$\frac{dX_{M_xO_y}}{dt} = -k_{sl}^{M_xO_y} \left(\frac{A}{V_{St}} \right) (X_{M_xO_y}^b - X_{M_xO_y}^*), \quad [27]$$

$$\frac{dX_M}{dt} = -k_m^M \left(\frac{A}{V_{St}} \right) (X_M^b - X_M^*). \quad [28]$$

The kinetics of desulphurization in the ladle are modeled similarly to oxidation. The only difference is that the interfacial concentrations are related by means of an equilibrium partition coefficient for desulphurization, L_S .

The model also takes into account the stirring effect, the effect of ladle furnace power on temperature, and change of composition due to alloying addition.

D. Flow Chart of the Calculation Program

The MATLAB[™] software was used to develop a computer code for solving the equations in this work. The algorithm employed is illustrated in Figure 5. First, composition of the molten steel and slag in addition to the number and size of inclusions is initialized. It is worth mentioning that there are two time loops for calculations. The outer loop for calculating change of composition due to the steel–slag reaction is shown by Δt and the inner loop for steel–inclusion reaction (dt). Since the processing conditions for the ladle are provided every 0.1 minutes and also slag–steel reactions occur more slowly than steel–inclusion reactions, $\Delta t = 60$ seconds and $dt = 1$ second are chosen for calculations in this work.

To calculate steel–slag interfacial concentrations, thermodynamic and kinetic parameters such as activities, thermodynamic equilibrium constants, and mass transfer coefficients should be determined. Temperature is also updated at this stage according to arcing or stirring conditions. Mass transfer coefficient of all the components in the molten steel is assumed to be equal

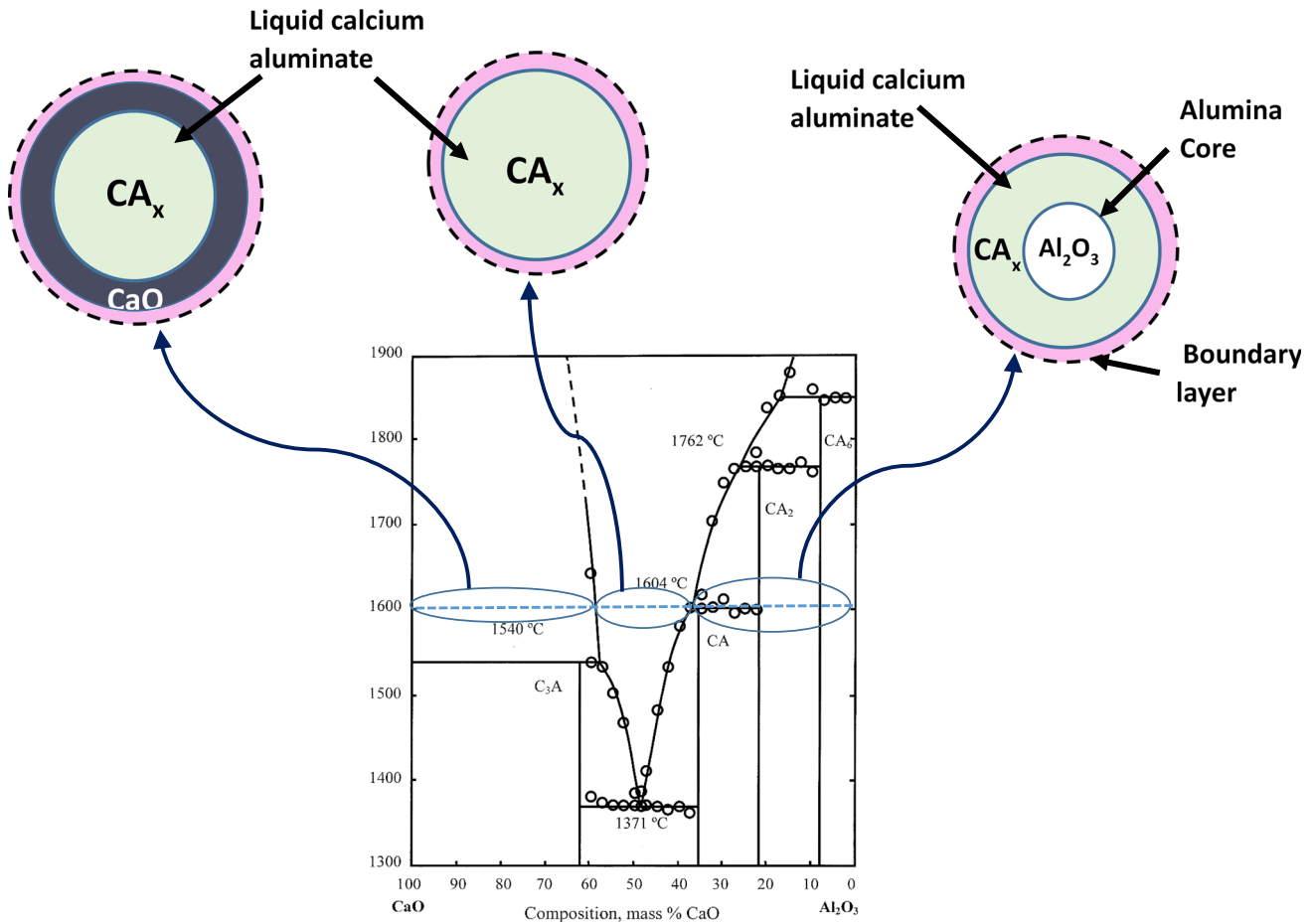


Fig. 4—Modification of alumina inclusion and corresponding phases.

and is determined by the empirical correlation with effective stirring power developed by Graham and Irons^[33,34]:

$$k_m = (0.06 \pm 0.002)\varepsilon^{1.4 \pm 0.09}, \quad [29]$$

where k_m is the volumetric mass transfer coefficient of the molten steel which includes the mass transfer coefficient, interfacial area between the metal and slag phase and volume of steel and ε is the effective stirring power (W/t).

The mass transfer coefficients of the components in the slag phase $k_{sl}^{M_xO_y}$ are calculated from individual ratios with the mass transfer coefficient of the species in steel $k_{sl}^{M_xO_y}/k_m^M$ which are the same as developed by Graham and Irons^[13] for this system.

After calculation of interfacial concentrations, the flux of each element in the steel and slag phase is calculated in each time step Δt . Then, the composition change of steel and slag is calculated. In the inner loop, first the calcium content of the steel is determined using the enhanced dissolution model described in Section II–A. To calculate the calcium dissolution rate, it is necessary to know the mass transfer coefficient at the calcium bubble boundary layer and the bubble interfacial area. These parameters are very difficult to measure, so in this study they are estimated based on work of Lu

et al.^[13] and fitting to the industrial heat. Steel–inclusion interfacial concentrations are calculated by considering mass balance and local thermodynamic equilibrium as explained in Section II–B–1. By knowing the interfacial concentrations, the flux of each component to the inclusions is calculated and hence the change of the composition of bulk steel and inclusions is calculated. Also the amount of sulfide and oxide inclusions produced is calculated.

III. RESULTS

In this section, the kinetic model is validated by comparison with data from an industrial heat of steel. The model can specifically calculate the following changes: (a) composition of components in the steel and the slag, (b) composition of component in the inclusions, and (c) the ratio of the oxide to sulfide inclusions.

A. Ladle Conditions

The initial chemical compositions of the steel and the slag at the beginning of ladle process used in the calculations are listed in Tables I and II and the operational conditions are shown in Table III, which

were obtained from the processing of a low-carbon aluminum-killed (LCAK) heat at ArcelorMittal Dofasco. In this heat, the Ca injection process was stopped every minute and the sample was taken for chemistry and inclusion analysis to have inclusion analysis during injection. To the authors' knowledge, such results have never been reported in the literature.

B. Inclusion Analysis

1. Number and size of inclusions

In this section, data from automated SEM analysis^[20] (ASPEX[®] Personal SEM Explorer with Metals Quality Analyzer) is used to determine the inclusion size and number for the model. The system classifies inclusions into different classes according to their compositions. The number of the various inclusions per unit volume of steel was calculated from automated SEM data using the Schwartz–Saltykov method^[35] as discussed in [Appendix](#). It was ensured that inclusions were not entrained slag based on their chemistry, size ($< 5 \mu\text{m}$), and morphology. All the inclusions used in this study were checked and entrained slag (if any) was removed from the data set for the analysis.

As mentioned earlier, an average size and number of alumina inclusions was chosen as the starting point for the model. As will be explained later, some calcium modification occurs before calcium injection, so the classes of inclusions which were the initial alumina at any time are CA_6 , CA_2 , CA , C_{12}A_7 , C_3A , and Al_2O_3 . [Table IV](#) shows the results for these classes. The resolution of the instrument is not fine enough to resolve the multi-layer structure, so that only the average composition is measured for individual inclusions. Typically 2000 to 3000 inclusions were counted in a 15 mm^2 sample. It is apparent that there are some variations in the distributions and sizes, but the average size and number at the bottom of [Table IV](#) represents a reasonable estimate of the average number and size of inclusions which were originally alumina.

CaS was also found in the samples, as well as CaMnS which forms from CaS during solidification. Inclusions containing Ca, S, and other minor elements such as Al, Mg, and Si were combined with CaMnS inclusions as other CaS inclusions in [Table V](#). The total number of sulfide inclusions dramatically increases during the injection process which strongly supports the enhanced dissolution model. Therefore, for the model it was assumed that the primary CaS inclusions that were formed according to enhanced dissolution were $1 \mu\text{m}$ diameter. The number of CaS inclusions was calculated in the model and compared with the measured numbers of sulfide inclusion in the results as a validation of the model.

[Table V](#) shows the average diameter and number of sulfide and oxide inclusions during injection.

Primary CaO inclusions may also have formed at the reaction plume; however, during injection the oxygen content of the steel was less than 5 ppm, and only very few very small CaO inclusions are likely to have formed. Thus, it is not surprising that none were detected by ASPEX. It is also likely that CaO inclusions were

dissolved in the water used during sample preparation for the SEM. The system found some unclassified inclusions with high Ca content. These results are labeled as “CaO” in [Table V](#), indicating that it is an assumed phase. Again, the numbers of “CaO” inclusions increase with injection time just as the CaS inclusions did. The numbers are much smaller than the sulfides, as would be expected by the enhanced dissolution model because there is much less dissolved O than S in the steel.

Less than 5 pct of the inclusions are spinel so the calcium associated with the spinel is negligible in comparison to alumina and sulfides in this specific heat. The authors recognize that spinel formation is common in ladle treatment and are currently working on an extension of the current model to include the modeling of calcium treatment of spinel inclusions.

2. Distribution of calcium sulfide and calcium aluminate inclusions

By knowing the diameter and the number of inclusions per unit volume of sulfide and calcium aluminate inclusions as shown in [Tables IV](#) and [V](#), the amount of Ca in each type of inclusion and subsequently total Ca may be calculated. [Figure 6](#) shows the distribution of Ca in the various inclusions during injection in comparison with the total Ca content measured independently by optical emission spectroscopy (OES). Total Ca by SEM is the total Ca in sulfide and calcium aluminate inclusions measured by SEM.

The total calcium content from automated SEM inclusion analysis is on average 21 pct below the total calcium content determined by OES, indicating that most of calcium is captured in the inclusion analysis. The major reason for the difference is thought to be the way inclusions are analyzed by automatic SEM. A size threshold is set that defines the smallest inclusion size that can be reliably counted, $0.5 \mu\text{m}$ in this case. Other researchers have also found that submicron inclusions are missed from SEM analysis.^[36] Also, since the size of the sample is usually small, occurrence of inclusions of clean steels is limited.^[37–39] It also can be due to loss of calcium oxides and sulfides during sample preparation.

[Figure 6](#) shows that most of the calcium reacts to form sulfide rather than calcium aluminates. It seems that calcium aluminate inclusions reach a saturated value and the rest of injected calcium contributes to form CaS inclusions.

For model calculations, a constant number of alumina/calcium aluminate inclusions is assumed as is the initial diameter. The latter is based on the average diameter of calcium aluminates from [Table IV](#). The effect of initial number and diameter of inclusions on transformation will be examined in detail in a future publication.

C. Species in the Steel

[Figure 7](#) shows the results of the model calculations for dissolved elements in the steel. Time zero was taken as the beginning of the ladle process after tapping. At 11 minutes, Al was added under strong stirring to

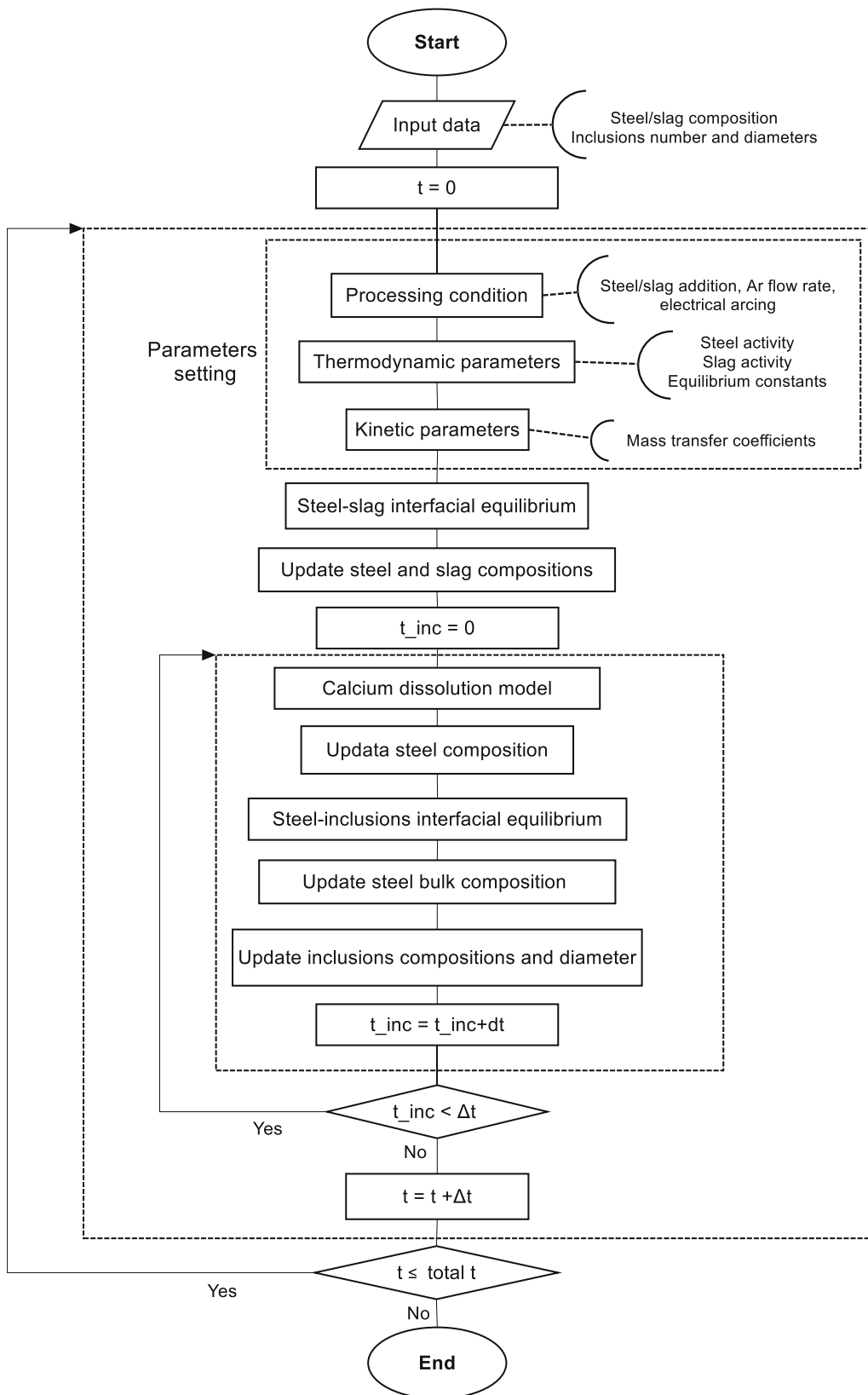


Fig. 5—Flow chart of the coupled steel-slag-inclusion kinetic model.

deoxidize the steel [Figure 7(c)] to promote desulfurization, but it also resulted in reversion of Mn and Si to the steel from the slag [Figures 7(a) and (b)]. There is very

good agreement between the model and the measured Mn, Si, and Al contents in the steel, just as there was in the original work used for the slag-metal model.^[40] A

Table I. Initial Steel Composition (Weight Percent)

C	Mn	P	S	Si	Al	N	Ca	O
0.0501	1.03	< 0.016	0.0123	0.063	0.0268	0.0045	0.00019	< 0.001

Table II. Initial Slag Composition (Weight Percent)

P ₂ O ₅	TiO ₂	CaS	FeO	CaO	MnO	SiO ₂	MgO	Al ₂ O ₃
0.09	0.44	0.425	1.15	42.4	0.56	13.56	12.86	28.34

Table III. Ladle Processing Conditions for Calculations

Initial Steel Temperature (K)	1867
Steel Mass (tonne)	164.5
Slag Mass (tonne)	2.58
Ladle Diameter (m)	3.2
Steel Height (m)	3.35
Slag Height (m)	0.127
Ar Flow Rate (Nm ³ /h/plug)	4 at low stirring regime and 25 at high stirring regime

second aluminum addition was made at 37 minutes, just before Ca wire injection. The very strong aluminum deoxidation drives the calculated dissolved oxygen to levels far below the limits of oxygen probes [Figure 7(e)]. With the very strong deoxidation, CaO is also reduced from the slag. The calculated dissolved Ca content is remarkably low in spite of the fact that the dissolved Ca content at the slag–metal interface during the high stirring rate is in the range of 0.003 to 0.005 ppm. Once the injection starts, the dissolved Ca content remains low [Figure 7(e)]. Both before and during injection, the dissolved Ca reacts very quickly with the inclusions, so the level remains low. It only climbs once the inclusion reactions are complete, approximately 4 minutes in Figure 7(e). At this time, the higher dissolved Ca drives the oxygen level very low [Figure 7(f)]. The reactions with the inclusions are discussed in the next section.

D. Inclusion Evolution

The change of composition of the calcium aluminate inclusions is presented in Figure 8. According to plant measurements, there is approximately 2 ppm Ca in the molten steel before injection. This is total calcium which is summation of calcium in inclusions and dissolved calcium in steel. However, the oxygen and sulfur content of the steel is high prior to aluminum addition, so the total calcium is likely present as some combination of calcium oxide and calcium sulfide, but evidently the CaO and CaS were too small to observe in the ASPEX. To test this hypothesis, the model was run assuming 2 ppm calcium was present in the steel prior to aluminum addition either CaS, CaO, or dissolved calcium. The results were identical in all three cases. When the aluminum is added, introducing alumina inclusions, they react with the calcium from these very fine inclusions. Because the calcium bearing inclusions are very small, this can happen in a few seconds, which explains the sharp jump right at the beginning of

aluminum addition seen in Figure 8(a). This result is consistent with the previous finding that if there is sufficient calcium available in the melt, inclusions will react to absorb all that calcium very quickly.^[12] The dissolved calcium from slag especially during the high stirring period is sufficient to partially modify alumina inclusions to calcium aluminate. Kumar and Pistorius^[13] also reported modification of alumina and spinel inclusions by calcium transferred from slag in laboratory scale. In another study, Shin and Park^[17] observed that the spinel inclusion changed entirely into a liquid oxide inclusion *via* the transfer of calcium from slag to metal in their experiments. There is remarkable agreement between the model prediction and the plant data regarding the extent of modification by this mechanism. Figure 8(b) shows that it takes approximately 3 minutes to modify alumina inclusions completely. At the end of the process, the calcium aluminate inclusions reach saturation level with CaO, and further inclusion reaction stops.

Figure 9 shows the relative abundance of sulfide and oxide inclusions, calcium aluminate inclusions, and total calcium in the molten steel. As oxygen concentration in the molten steel is much lower than sulfur, the amount of oxide inclusion produced at the injection zone is much lower than sulfide inclusions.

Total calcium is calculated by summation of the dissolved calcium and calcium in combination with sulfide, oxide, and calcium aluminate inclusions.

As mentioned above, one problem is estimating the $k_{Ca,L} \times A_{B,L}$ parameter, since measuring the bubble interfacial area is impossible. The $k_{Ca,L} \times A_{B,L}$ parameter was found to be in the range of $(1 \times 10^{-3} \text{ to } 10 \times 10^{-3})\text{S}^{-1}$ in the work of Lu^[41] in 40 kg steel heats by fitting the total calcium pickup to the enhanced dissolution model. According to the model, the total pickup rate is limited by availability of calcium, even though the recovery is much less than 100 pct. The total calcium content increases linearly with time because the

Table IV. Diameter and Number of Calcium Aluminate Inclusion During Calcium Injection

Time of Injection (min)	C ₃ A		C ₁₂ A ₇		CA		CA ₂		CA ₆		Al ₂ O ₃		Total Number of Calcium Aluminate Inclusions $\left(\frac{\times 10^{-12}}{\text{m}^3}\right)$	
	<i>d</i> (μm)	$N \left(\frac{\times 10^{-12}}{\text{m}^3}\right)$	<i>d</i> (μm)	$N \left(\frac{\times 10^{-12}}{\text{m}^3}\right)$	<i>d</i> (μm)	$N \left(\frac{\times 10^{-12}}{\text{m}^3}\right)$	<i>d</i> (μm)	$N \left(\frac{\times 10^{-12}}{\text{m}^3}\right)$	<i>d</i> (μm)	$N \left(\frac{\times 10^{-12}}{\text{m}^3}\right)$	<i>d</i> (μm)	$N \left(\frac{\times 10^{-12}}{\text{m}^3}\right)$		
0	1.14	0.77	1.06	2.8	1.43	6.5	1.50	9.6	0.82	0.87	1.35	0.89	20	
1.2	1.59	0.51	2.94	1.2	1.83	3.9	1.65	3.4	1.14	0.58	1.00	1.2	9.6	
2.2	1.22	1.6	2.31	1.8	1.78	5.9	1.01	7.2	4.05	0.17	0.80	4.2	17	
3.2	0.88	1.1	2.20	2.8	1.69	6.0	1.11	14.0	0.78	0.54	1.88	0.38	14	
4.3	0.96	3.1	3.18	2.2	1.60	4.3	1.31	2.4	0.00	0	1.40	0.44	12	
4.7	1.17	3.9	2.44	2.7	1.45	5.5	1.43	1.9	0.92	0.73	1.81	0.39	15	
Average														15

injection rate is constant. The same procedure is used here, yielding $3.7 \times 10^{-4} \text{ S}^{-1}$. The calcium injection rate was much higher in the industrial case, but the ladle size was even greater in scale resulting in an overall smaller value. The authors are carrying out further investigations using industrial heats to understand how $k_{\text{Ca,L}} \times A_{\text{B,L}}$ changes with injection conditions.

IV. DISCUSSION

These model results present a remarkably self-consistent explanation for the observed behavior in the full-scale ladle treatment for the dissolved species and the evolution of the inclusion composition. The most important aspect to appreciate is that there are a huge number of inclusions in the steel, so that if reactions with the inclusions are possible, then the bulk composition will respond immediately to the conditions. Thus, when aluminum is added to the steel, the oxygen content will quickly reach a low equilibrium value with alumina inclusions. A low oxygen content in the steel also permits reduction of CaO in the slag at the slag-metal interface. The dissolved Ca reacts very quickly with alumina, resulting in some alumina transformation before Ca injection. There is very close coupling between the slag and inclusions under these conditions. Once the Ca injection starts, there is a much faster supply of Ca resulting faster transformation. Thus, supply of Ca is rate-controlling for the inclusion transformations; diffusion in the inclusions is much faster. The model also provides a quantitative explanation for the timing and extent of the aluminate transformation, along with the CaS formation. The agreement of the model with the industrial data may be considered all the more remarkable when one considers that the only parameter fitted to the current data was the $k_{\text{Ca,L}} \times A_{\text{B,L}}$ for calcium in the bubble plume.

The previous model of transport for the inclusions^[20] that was used in the present model showed that diffusion in the liquid boundary layer and in the shrinking core layers was fast, and that the reactions were complete in a matter of seconds for a fixed bulk calcium content in the steel. Thus, the transformation is controlled by calcium availability, either from injection or the slag. Since those steps are so fast, they could be eliminated in the model as long as the proper boundary conditions for Ca, O, and Al are maintained at the inclusion interface.

There are some discrepancies between the model and the data (such as the dissolved Si and Al during injection) which could have been resolved by adjusting parameters, but that was not the objective of this work. The plant data presented in this paper represent the first heat that was studied using this model and more work is required to understand some of the details. In particular, the calcium injection provides strong stirring which should enhance the mass transfer rate, but it may also cause splashing and reduce the area of slag in contact with steel. These phenomena could result in reoxidation of steel.

As mentioned above and in a previous publication,^[12] the rate of supply of calcium to the melt is the

Table V. Diameter and Number of Sulphide and Oxide Inclusion During Calcium Injection

Time of Injection (min)	CaS		CaS Other		Total Number of Sulphide Inclusions ($\frac{\times 10^{-12}}{\text{m}^3}$)	CaO*	
	d (μm)	N ($\frac{\times 10^{-12}}{\text{m}^3}$)	d (μm)	N ($\frac{\times 10^{-12}}{\text{m}^3}$)		d (μm)	N ($\frac{\times 10^{-12}}{\text{m}^3}$)
0	0.00	0	0.98	19	19	0.00	0
1.2	0.65	2.3	0.84	43	46	0.00	0
2.2	0.94	5.4	0.94	100	110	0.00	0
3.2	0.99	2.4	0.93	170	190	2.56	0.28
4.3	1.05	56	0.96	160	220	1.05	0.61
4.7	1.26	57	1.39	860	140	1.51	0.43
Average	diameter (μm)		1.5			N ($\frac{\times 10^{-12}}{\text{m}^3}$)	0.44

*CaO is not classified in ASPEX® analysis. However, some unclassified inclusions of high Ca content assumed to be CaO.

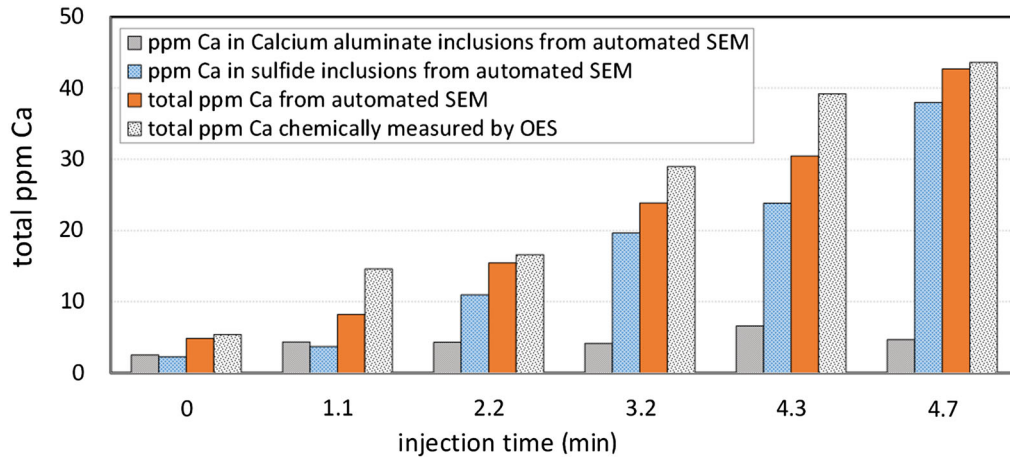


Fig. 6—Calcium distribution in different inclusions based on inclusion analysis result.

rate-controlling step for alumina transformation. It was argued^[12] that the instantaneous Ca content in the melt is the balance point between supply and consumption of Ca. During the strong stirring before the Ca injection, the rate of Ca supply *via* reduction of the slag was approximately 3.2×10^{-4} kg/s, which leads to an instantaneous Ca content of about 0.003 ppm. During the injection, the Ca supply rate was 2.1×10^{-2} kg/s, so the Ca content rose to approximately 0.1 ppm. Once the calcium aluminate inclusions reach saturation, the rate of calcium consumption decreases towards the end of injection and after all the oxygen is consumed the dissolved Ca increases.

As explained in a previous publication,^[12] the finding in the previous paragraph explains the fact that previous workers fitted various dissolved Ca contents to explain their results.^[12] Lu *et al.*^[7,10,16] were able to explain it rationally on the basis of the attained activities of sulfides, oxides, and dissolved sulfur and oxygen.

It should be noted that sulfide and oxide inclusions compete for the available calcium. First, as explained by the enhanced dissolution model, the diffusing Ca will react with S and O in the steel and the dissolved Ca can react with alumina inclusions for modification. So, the more S and O in the steel, the more CaO and CaS inclusions form at the reaction plane and less Ca is available for alumina inclusions which can delay

modification process. This finding explains the fundamental difficulty in making free-machining steel by adding sulfur to calcium-treated steel; any free calcium will quickly react to make solid CaS promoting nozzle clogging during casting.

Assuming that CaS inclusions are of uniform diameter, the number of CaS inclusions produced at the reaction plane is calculate using the first term in Eq. [22]. Table V shows that average size of sulfide inclusions is about 1 μm . Figure 10 shows the change of number of CaS inclusions during injection. There is good agreement between calculated result and plant data except the discrepancy at the end.

After steelmaking, LCAK steels are deoxidized (killed) with relatively large aluminum additions (0.01 to 0.06 pct Al). As mentioned earlier, the reaction between dissolved aluminum and oxygen is very rapid, resulting in dissolved oxygen contents in the range of 1 to 5 ppm and total oxygen contents in the range of 10 to 50 ppm in the form of alumina. In most results, as in the present work, the alumina inclusions are in the 1 to 10 μm range. The larger ones are eliminated rapidly by flotation and/or agglomeration. The smaller ones are below the limit of detection, but found to represent 10 to 20 pct of the total (see Figure 6). The present work provides a reasonable model for 80 pct of these inclusions. It appears that other phenomena such as inclusion

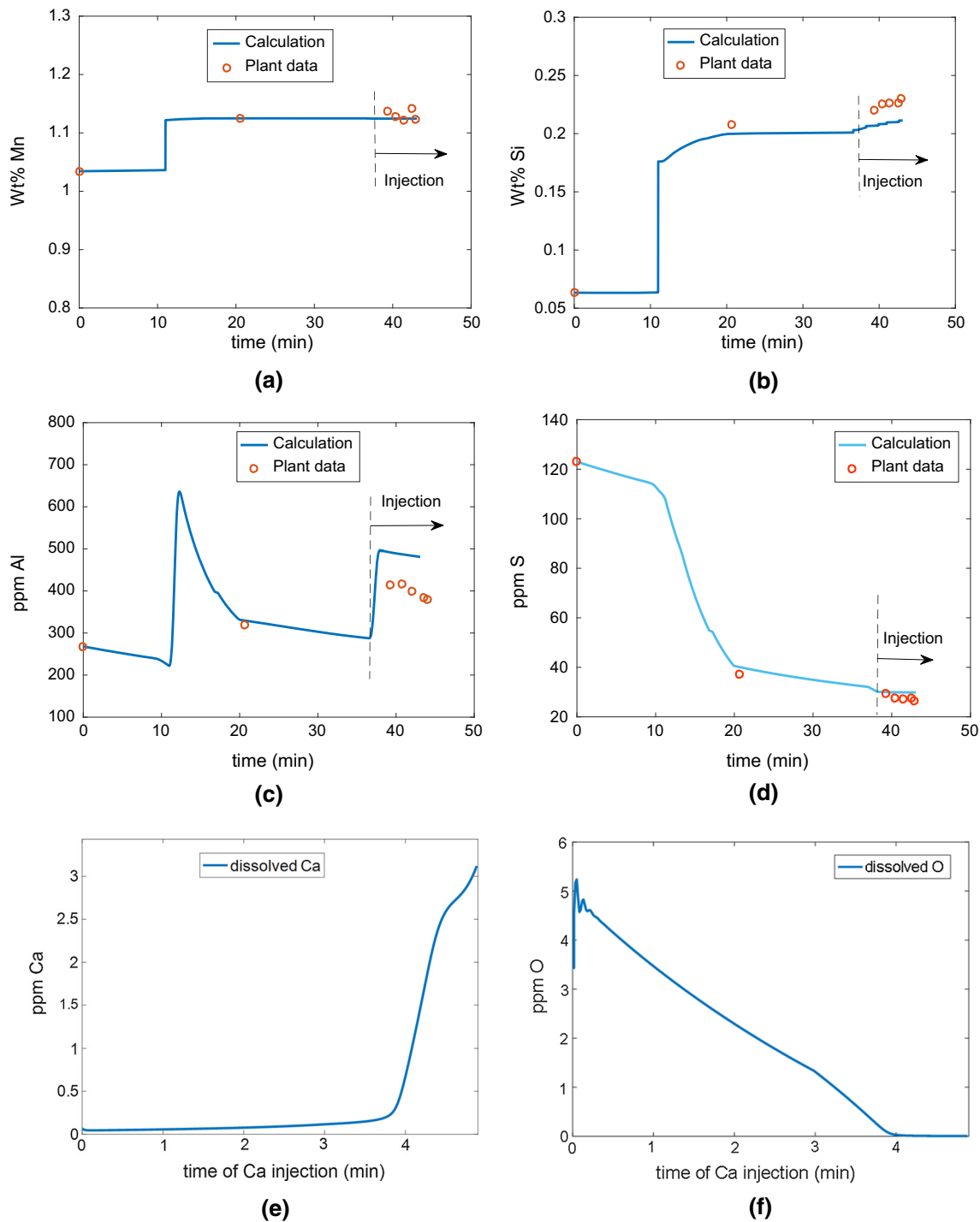


Fig. 7—Change of species in the steel during ladle process (a) Mn, (b) Si, (c) Al, (d) S, (e) Ca, and (f) O. Time zero for (a) through (d) is the beginning of ladle processing after tapping and time zero for (e) and (f) is the start of Ca injection, 38.3 min in (a) through (d).

agglomeration, flotation, and reoxidation do not have a significant effect. In a study by Kang *et al.*,^[42] samples were taken at different stages of ladle treatment and investigated by SEM. Also, inclusions were examined using a confocal scanning laser microscopy and found that alumina particles attracted each other and agglomerated. However, spinel inclusions and solid calcium aluminate inclusions did not show any sign of attraction or agglomeration. The other interesting finding of the

present work is that the primary oxide and sulfide inclusions are also in the range of 1 to 10 μm , possibly for the same reasons. Further work is underway to gather more evidence.

Because of the similarity of worldwide operations for LCAK steel, it is possible that the present model could be used very widely with only fine-tuning to local conditions. In a parallel study, also at ArcelorMittal Dofasco, Sun *et al.*^[7] found that the difference between

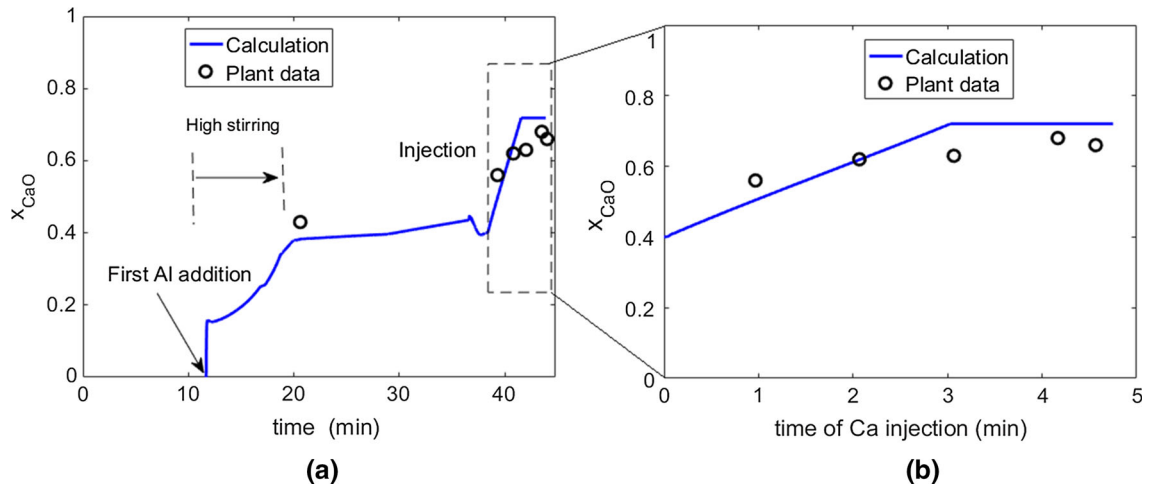


Fig. 8—Evolution of inclusions (a) and (b) calcium aluminate modification time zero for (b) through (d) is the start of Ca injection, 38.3 min in Fig. 7(a) through (d).

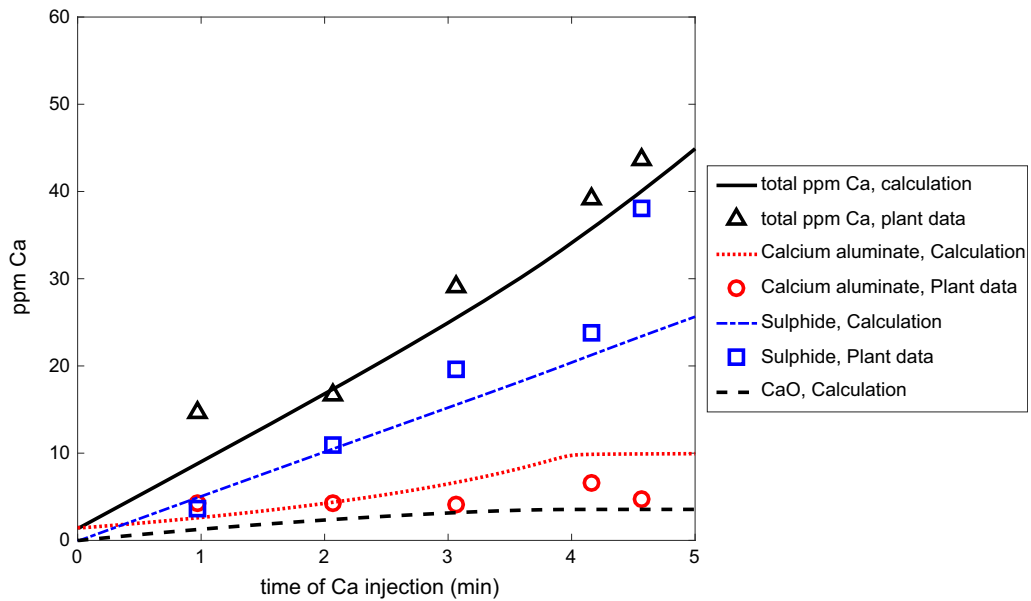


Fig. 9—CaS and CaO, calcium aluminate inclusions, and total calcium in the molten steel. Time zero is the start of Ca injection, 38.3 min in Fig. 7(a) through (d).

the total aluminum content and soluble aluminum in the steel was a good indicator of how much calcium was required for each heat. These analyses are rapid enough for process control. The current model also runs fast enough for process control as well. This avenue is under development in the McMaster Steel Research Centre with its industrial partners.

V. CONCLUSIONS

The aim of this work was to develop a kinetic model for the transformation of inclusions during calcium treatment and implementation of the steel-inclusion kinetic model to a previously developed kinetic model for the slag-steel reactions in the ladle metallurgy

furnace. Combining a calcium dissolution model with a shrinking core model for inclusion transformation and a slag-steel reaction model results in a fundamental kinetic model which allows determination of the change of composition of the steel, slag, and evolution of inclusions during Ca treatment. The coupled slag-steel-inclusion model shows that

- (1) Modification of alumina inclusions are controlled by the rate of supply of calcium because the inclusions consume the injected calcium so fast that the dissolved calcium reaches a fairly constant low value approximately 0.1 to 0.2 ppm during calcium treatment. This is highlighted by huge difference between dissolved calcium content of the steel compared to Ca reduced by the slag.

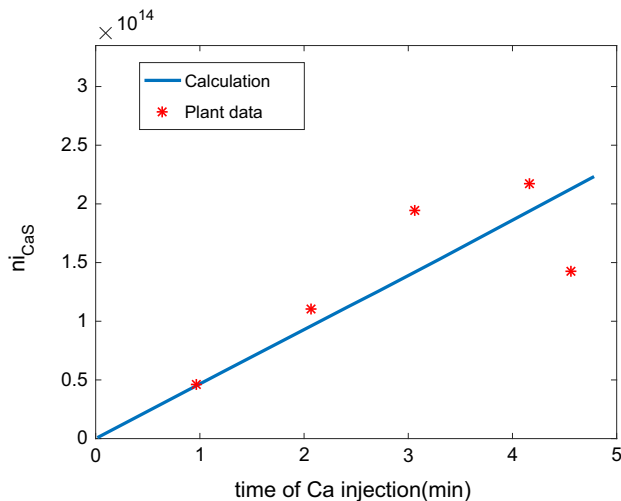


Fig. 10—Change of number of CaS inclusions. Time zero is the start of Ca injection, 38.3 min in Fig. 7(a) through (d).

- (2) The steel slag reactions is increased due to the calcium injection contribution to stirring in addition to that of argon.
- (3) Calcium transferred from the slag especially during high stirring period can be sufficient to partially modify alumina inclusions to calcium aluminatate.
- (4) By only considering CaS inclusions form at the injection plume, the model offers excellent prediction of sulfide formation suggesting that all CaS is formed at the plume.

ACKNOWLEDGMENTS

The authors are grateful for the support of the Members of the McMaster Steel Research Centre and the Natural Sciences and Engineering Research Council of Canada. The strong support and collaboration with ArcelorMittal Dofasco in planning and executing the work was vital.

APPENDIX: VOLUMETRIC SIZE DISTRIBUTIONS OF INCLUSIONS

An automated inclusion analysis SEM technique, ASPEX, was used to obtain planar distribution of inclusion on the polished section. Particle sizes are divided into number of size groups after they are measured on plane sections. The number and size of particles in the plane section is determined, but to obtain the size distribution on a volume basis, the analysis of the obtained data is required. It is assumed that the particles are spherical so that equivalent sphere diameters or equivalent circle diameters can be considered. ASPEX measures equivalent circle diameters of inclusions which can be presented in a particle size distribution histogram.

The number of circles per unit area N_A as a result of N_V spheres per unit volume of diameter D is

$$N_A = D \cdot N_V. \quad [AI]$$

So, larger spheres are more likely to be intersected by the plane of the polished section. Moreover, a sphere may be sectioned anywhere in its diameter. But, only largest spheres can lead to largest circle diameter at the sectioning surface. Therefore, the probability of spotting circles in this largest size group could be calculated and the residual probability distributed to the smaller size groups of circles. Then, circles from the next smallest size group of spheres are calculated and so on. Using this approach, the size distribution of spheres in the volume could be derived from the measurement of the size distributions of circles on the sectioning plane. The details of the method can be found in Reference 42. Schwartz^[36] and Saltykov^[43] developed a matrix of coefficients ($\alpha(i, j)$) for the number of circles in size group (i) arising from spheres in size group (j) using probability distributions for sectioning randomly distributed spheres of sizes in k equal size groups. The number of spheres per unit volume in size group j from the numbers of circles in size groups i is

$$N_V(j) = \frac{1}{\Delta} \{ \alpha(j, j)N_A(j) + \alpha(j, j+1)N_A(j+1) + \dots + \alpha(j, k)N_A(k) \}, \quad [AII]$$

where $j = 1$ to k , Δ is the size interval used in the histograms and k is the number of size groups.

REFERENCES

1. K.G. Rackers and B.G. Thomas: *78th Steelmak. Conf. Proc.*, Iron and Steel Society, Nashville, 1995, pp. 723–34.
2. S.W. Robinson, I.W. Martin, and F.B. Pickering: *Met. Technol.*, 1979, vol. 6, pp. 157–69.
3. L. Zhang and B.G. Thomas: *XXIV Natl Steelmak. Symp.*, Morelia, Mich, Mexico, 2003, pp. 138–83.
4. E.T. Turkdogan: *Fundamentals of Steelmaking*, 1st ed., Maney, London, 2010, pp. 285–90.
5. A. Ghosh: *Secondary Steelmaking: Principles and Applications*, 1st ed., CRC Press, London, 2001, pp. 203–17.
6. S. Basak, R. Kumar Dhal, and G.G. Roy: *Ironmak. Steelmak.*, 2010, vol. 37, pp. 161–68.
7. D. Lu, G.A. Irons, and W. Lu: *Ironmak. Steelmak.*, 1994, vol. 21, pp. 362–72.
8. Y. Higuchi, M. Numata, Sh. Fukagawa, and K. Shinme: *ISIJ Int.*, 1996, vol. 36, pp. 151–54.
9. Y. Ito, M. Suda, Y. Kato, H. Nakato, and K. Sorimachi: *ISIJ Int.*, 1996, vol. 36, pp. S148–50.
10. H. Visser, R. Boom, and M. Biglari: *ATS Int. Steelmak. Conf.*, 2008, pp. 172–80.
11. Z. Han, L. Liua, M. Lind, and L. Holappa: *Acta Metall. Sin.*, 2006, vol. 19, pp. 1–8.
12. Y. Tabatabaei, K.S. Coley, G.A. Irons, and S. Stanley: *Metall. Mater. Trans. B*, 2017, vol. 46B, pp. 2820–25.
13. K.J. Graham and G.A. Irons: in *Int. Symp. Highly Innov. Nov. Oper. "Future Steelmak. Metall."*, 2010, pp. 65–74.
14. A. Galindo, G.A. Irons, K.S. Coley, and S. Sun: in *Challenges Transform. Solut. Sustain. Steelmak. Cast. Environ. Metall. Innov. CTSSC-EMI Symp. 2015*, Tokyo, Japan, 2015.
15. A. Harada, N. Maruoka, H. Shibata, and Sh. Kitamura: *ISIJ Int.*, 2013, vol. 53, pp. 2110–17.
16. A. Harada, N. Maruoka, H. Shibata, M. Zeze, and N. Asahara: *ISIJ Int.*, 2014, vol. 54, pp. 2569–77.

17. D. Kumar and P.C. Pistorius: *Proc. 10th Int. Conf. Molten Slags, Fluxes Salts*, Wiley, Hoboken, NJ, USA, 2016, pp. 145–53.
18. J.H. Shin, Y. Chung, and J.H. Park: *Metall. Mater. Trans. B*, 2017, vol. 48B, pp. 46–59.
19. K. Graham: PhD Thesis, McMaster University, 2008, pp. 172–81.
20. D.-Z. Lu: PhD Thesis, McMaster University, 1992, pp. 206–29.
21. O. Levenspiel: *Chemical Reaction Engineering*, 2nd ed., Wiley, New York, 1999, pp. 570–77.
22. N. Verma, P.C. Pistorius, R.J. Fruehan, M.S. Potter, H.G. Oltmann, and E.B. Pretorius: *Metall. Mater. Trans. B*, 2012, vol. 43B, pp. 830–40.
23. N. Verma, P.C. Pistorius, R.J. Fruehan, and R.J. Lee: in *Mater. Sci. Technol. Conf. Exhib. 2009, MS T'09*, Pittsburgh, PA, 2009, pp. 1042–53.
24. S.F. Yang, J.Sh. Li, Z.F. Wang, J. Li, and L. Lin: *Int. J. Miner. Metall. Mater.*, 2011, vol. 18, pp. 18–23.
25. J. Szekely and N.J. Themelis: *Rate Phenomena in Process Metallurgy*, 1st ed., Wiley-Interscience, New York, 1971.
26. F. Oeters: *Metallurgy of Steelmaking*, 1st ed., Verlag Stahleisen, Düsseldorf, 1994.
27. C.W. Bale, P. Chartrand, S.A. Degterov, G. Eriksson, and K. Hack: *Calphad*, 2002, vol. 26, pp. 189–228.
28. C.W. Bale, E. Bélisle, P. Chartrand, S.A. Decterov, G. Eriksson, K. Hack, I.-H. Jung, Y.-B. Kang, J. Melançon, A.D. Pelton, C. Robelin, and S. Petersen: *Calphad*, 2009, vol. 33, pp. 295–311.
29. M. Hino and K. Ito: *Thermodynamic Data for Steelmaking*, 1st ed., Tohoku University Press, Tokyo, 2010, pp. 16–17.
30. H. Fujiwara, A. Hattori, and E. Ichise: *Tetsu-To-Hagane/J. Iron Steel Inst. Jpn*, 1999, vol. 85, pp. 201–07.
31. Q. Han, X. Zhang, D. Chen, and P. Wang: *Metall. Mater. Trans. B*, 1988, vol. 19B, pp. 617–22.
32. D.G.C. Robertson, B. Deo, and S. Ohguchi: *Ironmak. Steelmak.*, 1984, vol. 11, pp. 41–55.
33. M. L. Kapoor and M. G. Froberg: in *Chem. Metall. Iron Steel*, 1971, pp. 17–22.
34. H. Gaye and J. Welfringer: in *Second Int. Symp. Metall. Slags Fluxes*, 1984, pp. 357–75.
35. F. Schamber: *Introduction to Automated Particle Analysis by Focused Electron Beam*, 2009.
36. R. Higgison and C.M. Sellars: *Worked Examples in Quantitative Metallography*, 1st ed., Maney, London, 2003, pp. 68–76.
37. P. Kaushik, H. Piolet, and H. Yin: *Iron Steel Technol.*, 2009, vol. 6, pp. 82–99.
38. N. Verma, P.C. Pistorius, R.J. Fruehan, M. Potter, M. Lind, and S. Story: *Metall. Mater. Trans. B*, 2011, vol. 42B, pp. 711–19.
39. M. Nuspl, W. Wegscheider, J. Angeli, W. Posch, and M. Mayr: *Anal. Bioanal. Chem.*, 2004, vol. 379, pp. 640–45.
40. B.G. Bartosiaki, J.A.M. Pereira, W.V. Bielefeldt, and A.C.F. Vilela: *J. Mater. Res. Technol.*, 2015, vol. 4, pp. 235–40.
41. J.H. Shin and J.H. Park: *Metall. Mater. Trans. B*, 2017, vol. 48B, pp. 2820–25.
42. S. Sun, S. Waterfall, N. Strobl, D. Liao, and D. Holdridge: in *8th Int. Symp. High-Temperature Metall. Process.*, 2017, pp. 347–57.
43. H.A. Schwartz: *Met. Alloy*, 1934, vol. 5, pp. 139–40.